THE BRAGG CRYSTAL SPECTROMETER FOR SOLAR-A*

J. L. CULHANE[1], E. HIEI[2], G. A. DOSCHEK[3], A. M. CRUISE[4], Y. OGAWARA[5], Y. UCHIDA[6], R. D. BENTLEY[1], C. M. BROWN[3], J. LANG[4], T. WATANABE[2], J. A. BOWLES[1], R. D. DESLATTES[7], U. FELDMAN[3], A. FLUDRA[1], P. GUTTRIDGE[1], A. HENINS[7], J. LAPINGTON[1], J. MAGRAW[4], J. T. MARISKA[3], J. PAYNE[4], K. J. H. PHILLIPS[4], P. SHEATHER[1], K. SLATER[4], K. TANAKA[2]**, E. TOWNDROW[4], M. W. TROW[1], and A. YAMAGUCHI[2]

Abstract. The Bragg Crystal Spectrometer (BCS) is one of the instruments which makes up the scientific payload of the SOLAR-A mission. The spectrometer employs four bent germanium crystals, views the whole Sun and observes the resonance line complexes of H-like Fe XXVI and He-like Fe XXV, Ca XIX, and S XV in four narrow wavelength ranges with a resolving power ($\lambda/\Delta\lambda$) of between 3000 and 6000. The spectrometer has approaching ten times better sensitivity than that of previous instruments thus permitting a time resolution of better than 1 s to be achieved. The principal aim is the measurement of the properties of the 10 to 50 million K plasma created in solar flares with special emphasis on the heating and dynamics of the plasma during the impulsive phase. This paper summarizes the scientific objectives of the BCS and describes the design, characteristics, and performance of the spectrometers.

1. Introduction

The solar flare problem represents one of the most difficult challenges posed in astrophysics. In the past 15 years it has become clear that progress can best be made with the aid of observations throughout the widest electromagnetic spectrum. The Bragg Crystal Spectrometer (BCS) will be used at X-ray wavelengths to study plasma heating and dynamics particularly during the impulsive phase of solar flares. The emission lines selected for observation allow the measurement of plasma velocity, temperature, and emission measure. Study of these flare plasmas will be undertaken jointly by all the SOLAR-A instruments. The measurement of element abundances and abundance variations will be an important aim of BCS observations in particular.

High spectral and temporal resolution coupled with high sensitivity are necessary features of an instrument designed to achieve the above objectives. The BCS will have almost ten times greater sensitivity than was available from the instruments flown on SMM (Acton *et al.*, 1980), P78–1 (Doschek, 1983) and HINOTORI (Kondo, 1983) during the last solar maximum. It will employ fixed bent crystals with one-dimensional

[1] Mullard Space Science Laboratory, University College London, Holmbury, U.K.
[2] National Astronomical Observatory of Japan, Tokyo, Japan.
[3] US Naval Research Laboratory, Washington, D.C., U.S.A.
[4] Rutherford Appleton Laboratory, Abingdon, U.K.
[5] Institute of Space and Astronautical Science, Tokyo, Japan.
[6] University of Tokyo, Tokyo, Japan.
[7] National Institute for Standards and Technology, Washington, D.C., U.S.A.

* After the launch the name of SOLAR-A has been changed to YOHKOH.
** Tragically Professor K. Tanaka died on January 2, 1990.

Solar Physics **136:** 89–104, 1991.

position-sensitive proportional counters to register the spectra. The spectral resolution will be comparable to that of the similar instrument on SMM but the enhanced sensitivity will permit a time resolution of better than 1 s. A flexible on-board data processing system, including a large queue memory, will allow a wide range of operating modes to be implemented during the mission.

In the rest of the paper the scientific aims of the BCS are summarized, the design of the spectrometers is described with particular reference to the Bragg crystal performance, the X-ray detectors and the on-board processor. A brief account will be given of the instrument calibration. We must emphasize that the instrument performance parameters presented are preliminary in nature and require verification following *in-orbit* operation. They should not be used for data analysis. A users manual is being prepared and will be updated after the launch of SOLAR-A.

2. Scientific Objectives

Following the impulsive release of energy in a solar flare, a large quantity (emission measure $\simeq 10^{48}$–10^{50} cm^{-3}) of high temperature ($T \simeq 10$–50×10^6 K) plasma is created. The manner of the plasma creation and the dynamics and other properties of the high-temperature gas all provide essential clues to understanding the flare mechanism. In the above temperature range the high-ionization stages (e.g., H-like and He-like) of abundant elements are formed and the plasma properties may be studied by observing the X-ray emission spectra of these ions. The sensitivity and wavelength resolution of the spectrometers permit line intensities and profiles to be measured with sufficient time resolution to obtain detailed observations throughout the impulsive phase of flares. The data will be used in the following investigations:

Plasma dynamics. Observations with high-resolution X-ray spectrometers during the past decade have demonstrated that the emission lines are significantly broadened during the flare impulsive phase. The 'turbulent' width, substantially greater than the Doppler width implied by simultaneous electron temperature measurement, indicates mass motion velocities approaching 200 km s^{-1} (Doschek *et al.*, 1980; Antonucci *et al.*, 1982). There may also be a correlation of non-thermal line width with associated hard X-ray flux. In addition the broadening may be non-random on short time scales (Doyle and Bentley, 1987; Fludra *et al.*, 1989). A blue-shifted component is often observed for disc flares (Doschek *et al.*, 1980; Feldman *et al.*, 1980; Antonucci *et al.*, 1982) indicating upward moving plasma with velocity of 300 km s^{-1} or greater. This plasma has been attributed to 'chromospheric evaporation' – the ablation of plasma heated by energy transported form the flare site (Antonucci *et al.*, 1982; Antonucci, Gabriel, and Dennis, 1984) but the details of this process and of the energy transport mechanism, remain controversial. Use of the enhanced sensitivity and time resolution of the SOLAR-A BCS will lead to major advances in this important area of flare physics.

Plasma heating and diagnostics. There is significant evidence from previous observations that heating and turbulence occur even before the impulsive phase of the flare. The increased sensitivity of the BCS will permit early measurement of temperature with

much increased statistical precision. It will also be possible to search for anomalous line ratios which will indicate transient ionization effects thus allowing the estimation of electron densities in the range below 10^{11} cm^{-3}. Greater sensitivity will permit improved estimation of plasma parameters such as temperature and emission measure. Comparison of these measurements with Soft X-ray Telescope (SXT) images which are expected to have better than 3 arc sec spatial resolution will allow the direct estimation of electron density and the determination of differential emission measure over a wide temperature range.

Superhot component. Observations of the H-like iron (Fe XXVI) emission line spectrum will be particularly important for the study of the plasma at temperatures of around 50×10^6 K that is detected in some flares (Lin *et al.*, 1981; Tanaka *et al.*, 1982). Temperatures will be obtained from the intensity ratio of the Fe XXV dielectronic lines to those of the Fe XXVI Lα lines. In addition it will be possible for the first time to obtain statistically significant profiles for the Lα lines and so investigate the dynamics of this important component. Data from HINOTORI (Tanaka, 1987) provided a tentative indication of variability in the Fe XXVI line profiles. The enhanced spectral resolution of the BCS will permit detailed observations of line profile variations with time.

Flare decay phase. Although the main release of energy in the flare occurs during the impulsive phase, there is evidence for continued energy injection during the decay phases of some flares. The BCS will permit a detailed study of this process. For large limb flares, it may be possible to observe the increase in height of the emitting plasma since spatial displacement translates into spectral displacement in the BCS. Such plasma, contained in large post-flare loops, was observed with the SMM BCS to have a temperature of $\simeq 5$–6×10^6 K many hours after the flare had occurred (Švestka *et al.*, 1982). Combined observations by the SXT and the BCS will allow a substantial advance in this area. Finally the measurement of line to continuum ratios during flare decay will allow flare-to-flare abundance variations to be studied for a range of elements (Sylwester, Lemen, and Mewe, 1984; Sylwester, 1987).

3. Design of the SOLAR-A Bragg Crystal Spectrometer System

The crystal spectrometers constructed for flight on SOLAR-A are similar to those successfully launched on the Solar Maximum Mission (Rapley *et al.*, 1977; Acton *et al.*, 1980). In the case of SOLAR-A however the presence of high-quality imaging X-ray telescopes, the smaller mass and volume available, and the results obtained by the SMM have led to a somewhat different approach to the instrument design.

Conventional Bragg spectrometers scan in wavelength by rotating a flat crystal so that a range of angular positions (θ) converts a range of wavelengths (λ) according to Bragg's law $n\lambda = 2\,d \sin\theta$. For SOLAR-A each spectrometer crystal is curved with a fixed radius so that a parallel beam of solar X-rays is incident at a range of Bragg angles θ_1 to θ_2. Diffracted radiation, at corresponding wavelengths λ_1 to λ_2, is registered in a one-dimensional position-sensitive proportional counter (see Figure 1). Given the existence of the imaging X-ray telescopes, the small probability of simultaneous flare

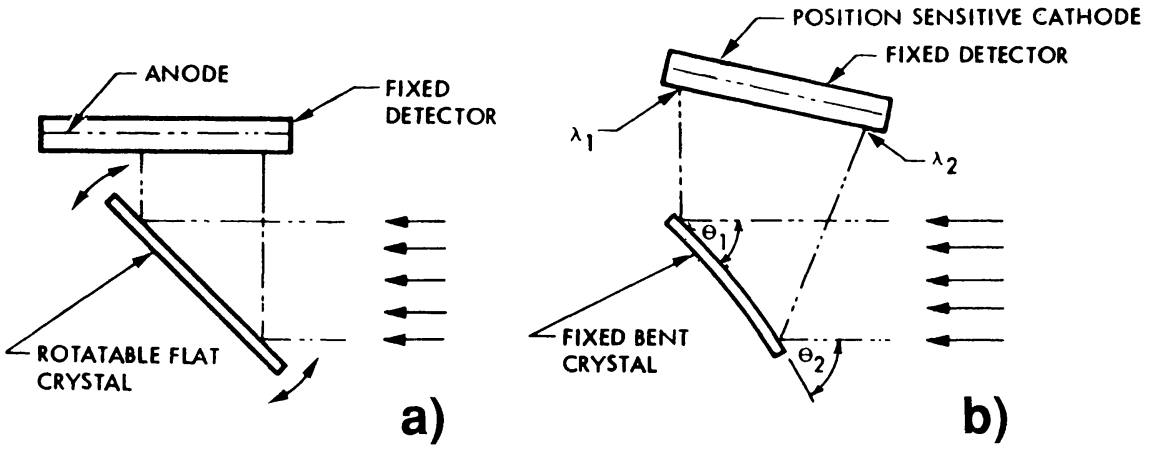

Fig. 1. Schematic diagram of (a) flat scanning crystal spectrometer and (b) fixed bent crystal spectrometer.

occurrence in different active regions and the relatively small mass and volume available for the BCS, a multi-grid collimator was not employed on SOLAR-A and so the BCS views the entire solar disc. This, coupled with increased crystal area, allows a factor approaching ten increase in sensitivity relative to the SMM instrument. The sensitivity of a bent crystal spectrometer can be obtained from the relation given by Rapley *et al.* (1977) as

$$S = [T_w T_f F_b \eta_d A_p R_c]/\Delta\theta, \tag{1}$$

where S is the sensitivity in cm^2, T_w and T_f are the transmissions of the detector window and the thermal filter, F_b is the fractional detector area lost due to the window support bars, η_d is the X-ray absorption efficiency of the detector gas, A_p is the projected area of the crystal in cm^2, R_c and $\Delta\theta$ are the integrated reflectivity of the crystal and the range of incident Bragg angles, both in radians.

From (1) S is inversely proportional to $\Delta\theta$ and therefore to the wavelength range $\lambda_2 - \lambda_1$ covered by each crystal. In order to maximize S it is therefore necessary to select the minimum wavelength range that is consistent with achieving the scientific aims. However, since Bragg angle range translates to wavelength range, the minimum spectral coverage must be increased to allow for uncertainties in spacecraft pointing, for spectrometer alignment errors, and for the range of flare locations on the surface of the Sun. With the crystal dispersion direction aligned approximately perpendicular to the solar equator, the allowance of an addtional $\pm$ 12 arc min in Bragg angle permits the chosen spectral ranges to be registered for all possible spacecraft pointing directions which lie inside a circle of 5 arc min angular radius about Sun centre and for most flares which occur mainly in a latitude range of $\pm$ 7 arc min about the equator.

The BCS employs four bent crystals to cover selected wavelength ranges of diagnostic importance. These ranges are shown in Figure 2 superimposed on spectra of Fe XXVI taken from HINOTORI data (Tanaka, 1987), Fe XXV and Ca XIX taken from SMM BCS data (Culhane *et al.*, 1981) and S XV taken from SMM Flat Crystal Spec-

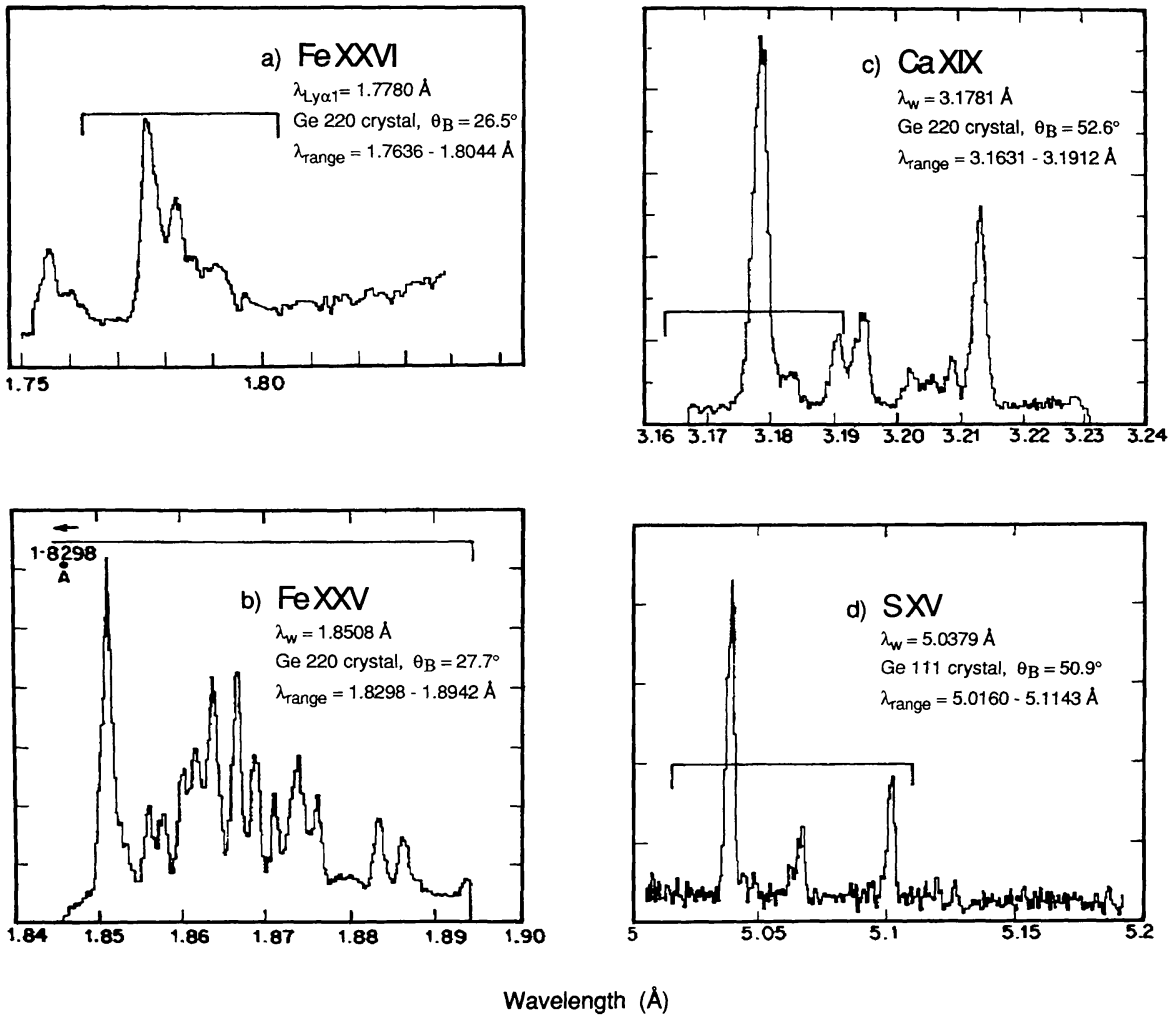

Fig. 2. Bragg crystal spectra of solar flares. (a) Fe XXVI obtained with HINOTORI, (b) Fe XXV and (c) Ca XIX obtained with the SMM bent crystal spectrometer, and (d) S XV obtained with the SMM flat crystal spectrometer. The solid lines indicate the spectral coverage for the four SOLAR-A spectrometers. See text for references.

trometer (FCS) data (Acton *et al.*, 1981). The Fe XXVI range will permit velocity and temperature measurements for the superhot component. Coverage of the Ca XIX range has been essentially restricted to the resonance transition to allow velocity measurements at maximum resolution and sensitivity. However, there is some temperature information available from the intensity of the n = 3 satellite lines that fall close to the long wavelength side of the resonance line. The more complete coverage of the Fe XXV and S XV ranges will permit both velocity and temperature measurements.

The four crystals are mounted in two structures as shown in Figure 3. X-rays from the Sun (Z-direction) enter the open apertures of the spectrometers through a pair of thin aluminized Kapton thermal filters (not shown in the figure) which are mounted over openings in the front panel of the spececraft. The incoming radiation strikes the crystals which are curved and fixed in place before launch so as to cover the selected wavelength ranges. The radiation is then diffracted into detectors located inside each structure. The

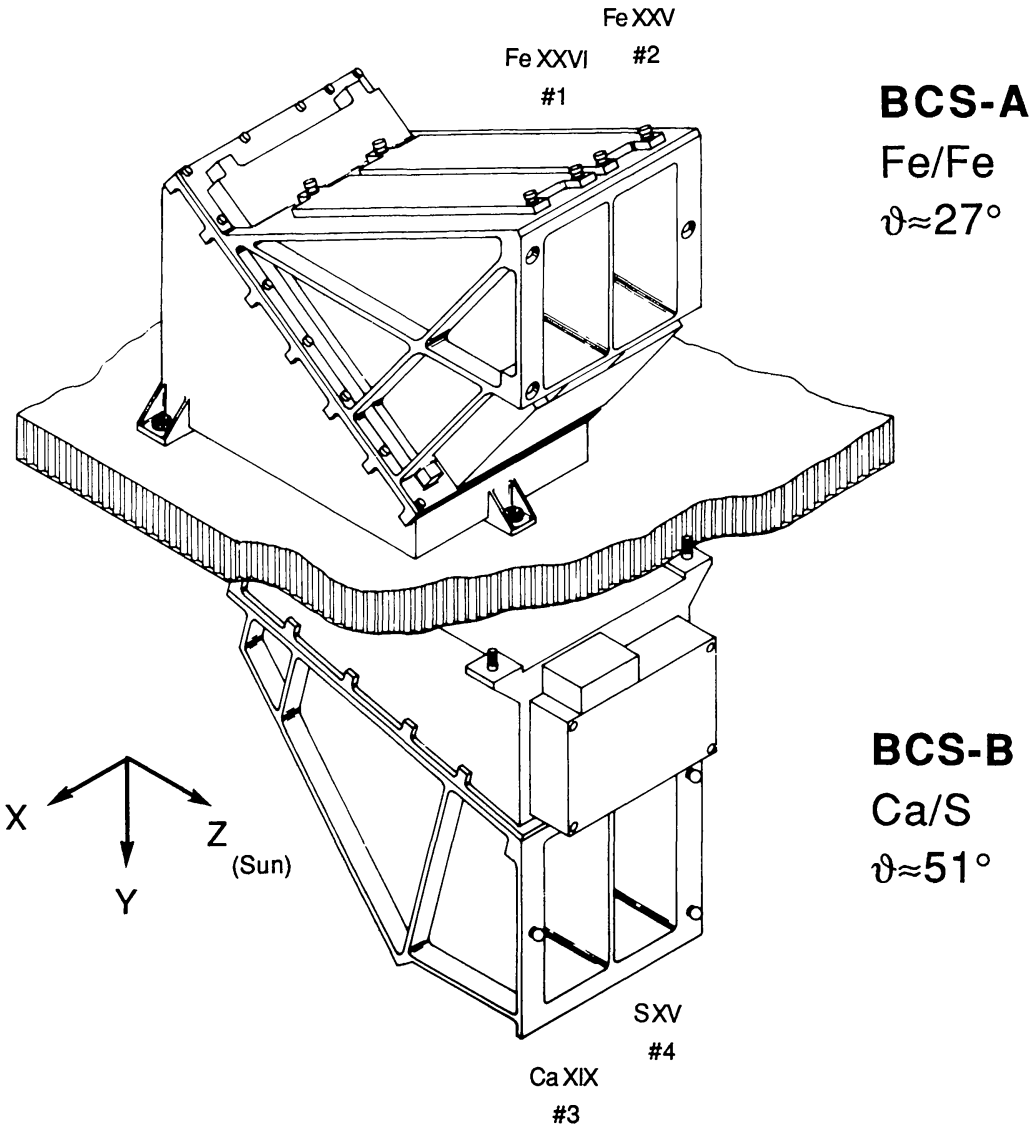

Fig. 3. Isometric views of the two SOLAR-A spectrometers. The units are mounted on opposite sides of the spacecraft centre panel.

only moving parts are two stepper motors which can rotate to admit 5.89 keV Mn–K X-rays from Fe^{55} radioactive sources to the detectors to enable their gas gain and energy resolution to be measured in flight.

Within the spectrometers an optical technique is used to set each crystal at the appropriate Bragg angle with a precision of better than $\pm$ 15 arc sec with respect to the plane defined by the feet of the spectrometers. Each spectrometer has three feet with precisely located and sized screw holes to enable accurate mounting on the spacecraft centre panel. Precision shoulder screws attach the feet to the centre panel. An optically located drill template is used to position the mating holes in the centre panel in the correct relationship to the Z-axis of the spacecraft. The openings in the centre panel mounting holes are accurately reamed to accept the barrels of the shoulder screws. Clearances of 25 μm are maintained so that the shoulder screws serve both as attach-

ments and as locating pins. The alignment procedure ensures that the optical axis of the BCS is co-aligned with the Z-axis of the spacecraft. As the centre panel is specified to be flat to within ± 3.4 arc min, provision is made for shimming the spectrometer during mounting on the spacecraft to optimize the Bragg angle ranges.

The two spectrometer units, labelled BCS-A and BCS-B, each contain two germanium crystals which have been paired so as to have approximately the same Bragg angles. The spectrometer structures are built with reference surfaces having the average of the two Bragg angles machined into the crystal support structure. Each crystal mount has three mounting pads that can be ground to ensure that the crystal offers the required range of Bragg angles to incoming solar radiation. The crystal mounts are made from titanium whose thermal expansion coefficient is well matched to that of germanium. The front surfaces of the mounts are ground to a concave cylindrical shape of the required radius. The 0.6 mm thick crystals are bent to the correct curvature and then attached to the mount with epoxy.

The crystal parameters and the wavelength ranges covered are listed in Table I. The crystals are somewhat larger than those flown on earlier missions. While Ge (220) crystals were used in both the P78–1 and SMM spectrometers, the Ge (111) crystal has not been flow previously. Before mounting in the spectrometer each crystal was characterized by measurements of its curvature and integrated reflectivity using X-rays.

The BCS instrument response is summarized in Table II. The wavelength resolution is set by the geometry of the spectrometers, the crystal rocking curves and the X-ray position resolution of the detectors. Each detector has a single position encoding arrangement – a modified wedge and strip pattern. X-rays from pairs of crystals are registered in each detector and are identified by signals from separate anode wires. The operation and performance of the detectors is dealt with in the next section.

Spectra are accumulated in the on-board digital processing system for a fixed time interval after which the total count in each spectral bin is compressed to an 8-bit number. At the flare-mode telemetry rate of 2 kbits s^{-1} for the BCS, four complete spectra can be transmitted every 4 s. However, the digital system incorporates a large queue memory which can be filled with spectra at a faster rate for later transmission. For example, the spectrometer can store a series of four spectra with 1 s time resolution for up to 7 min thus acquiring a total of 420 sets each of four spectra. This mode of operation can be initiated by an on-board flare occurrence flag thus enabling spectra to be acquired at higher time resolution during the impulsive phase. The digital data system will be described more fully in Section 5.

4. Detectors and Analogue Electronics

An exploded view of the one-dimensional position-sensitive proportional counter is given in Figure 4. The detector is filled with a mixture of Ar and Xe both at 47.5% with CO_2 (5%) as a quench gas to an overall pressure of 1.2 atm. The body is in two stainless steel halves. A beryllium foil window of 125 μm thickness is brazed to the upper section while the anodes, cathodes, and readout pattern are installed in the lower section. The

TABLE I

Ions, crystal parameters, and wavelength ranges

Channel No.	Ion	Resonance line λ (Å) (Bragg angle)	$2d$ (Å)	Crystal (rocking curve)	Crystal bend radius (m)	Wavelength range (Å) ($\Delta\theta$, mrad)	Crystal size (cm)	R_c (μrad)
BCS-A								
1	Fe XXVI	1.7780 (26.39°)	4.000	Ge 220 (14 arc sec)	13.64	1.7636–1.8044 (11.40)	3.98 × 18.1	67
2	Fe XXV	1.8509 (27.56°)	4.000	Ge 220 (15 arc sec)	10.20	1.8298–1.8942 (18.19)	3.98 × 18.1	68
BCS-B								
3	Ca XIX	3.1769 (52.58°)	4.000	G2 220 (50 arc sec)	9.60	3.1631–3.1912 (11.57)	3.98 × 11.4	116
4	S XV	5.0385 (50.46°)	6.532	Ge 111 (68 arc sec)	4.56	5.0160–5.1143 (23.83)	3.98 × 11.4	121

TABLE II

BCS instrument response

Channel No.	Ion	Wavelength range (Å)	Wavelength resolution		Thermal Doppler width FWHM (mÅ)	T_{ion} (10^6 K)	Sensitivity	
			(mÅ)	($\lambda/\Delta\lambda$)			S (cm^2)	SOLAR-A/SMM
BCS-A								
1	Fe XXVI	1.7636–1.8044	0.38	4700	1.20	50	0.15	9 [a]
2	Fe XXV	1.8298–1.8942	0.53	3500	0.90	25	0.10	9 [a]
BCS-B								
3	Ca XIX	3.1631–3.1912	0.53	6000	1.60	20	0.20	6 [a]
4	S XV	5.0160–5.1143	1.86	2700	2.50	15	0.04	63 [b]

[a] SMM bent crystal spectrometer.

[b] SMM flat crystal spectrometer scanning the S XV resonance line at 10 arc sec.

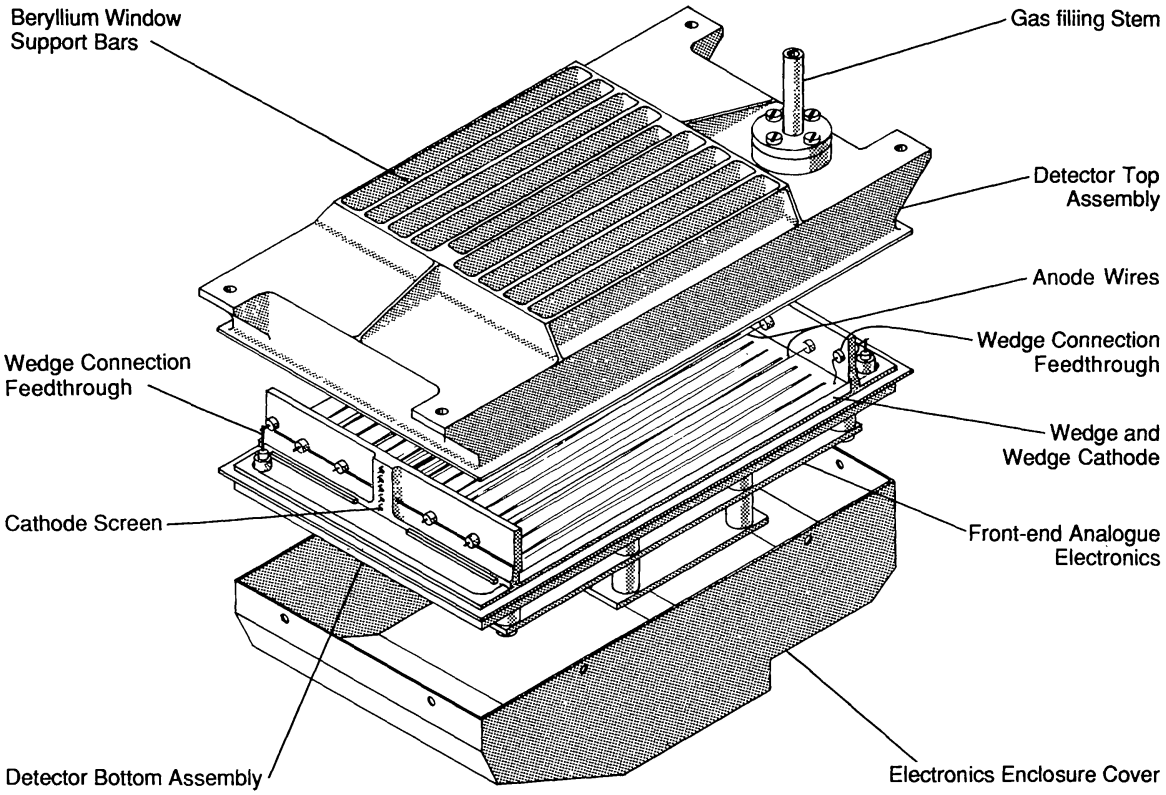

Fig. 4. An exploded view of the double proportional counter. A single one-dimensional position readout pattern is common to both halves. Each half detector registers X-rays from a single crystal and has two connected anode wires. The two halves are electrically separated by a screen of cathode wires. The top and bottom assemblies are sealed together by electron beam welding.

two sections are then sealed together by electron beam welding. The detector has two pairs of 15 μm dia. anode wires separated by a cathode screen of 9 grounded 25 μm dia. wires. Each pair of anodes is connected to a separate pre-amplifier. Thus X-rays from each of the two crystals can be registered separately. Anodes are maintained at a potential of ~ 1.5 kV by a high voltage unit (HVU). In order to monitor the gain and energy resolution of each detector, a 32-channel diagnostic pulse-height analyzer (PHA) is available (Figure 5) whose input can be switched to any one of the four detector channels. Used in conjunction with the on-board Fe^{55} calibration sources, the PHA allows detector performance to be checked during spacecraft night.

The double-wedge readout pattern is shown schematically in Figure 5. It is manufactured photolithographically on a gold-coated fused silica plate. The substrate material is chosen for low dielectric constant so as to minimize the capacitance between the two sets of gold wedge electrodes. This ensures low noise in the wedge 1 (W1) and wedge 2 (W2) pre-amplifiers. Following the absorption of an X-ray photon, a charge avalanche occurs on one of the anode wires and the induced charge distribution on the two interlocking wedge electrodes provides the event position determination. If Q_{W1} and Q_{W2} are the induced charges on each electrode then the one-dimensional position

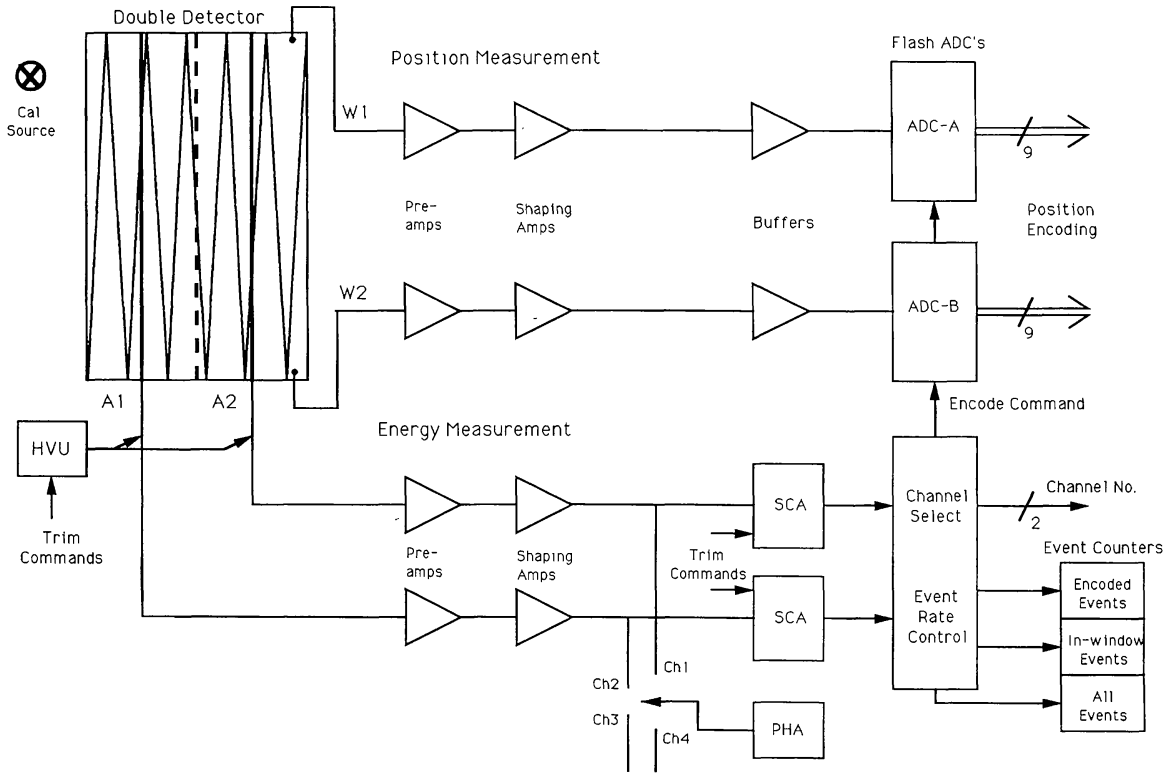

Fig. 5. A schematic diagram of the X-ray event processing electronics. Signals from the two wedge patterns (W1 and W2) are amplified and passed to 9 bit analogue-to-digital converters. Anode signals (A1 and A2) from the double detector are amplified and passed to single channel analysers (SCA). A switch-selectable pulse height analyser (PHA) can examine the X-ray events from each anode of the two double detectors. Each detector has its own high voltage unit (HVU).

coordinate for the X-ray event is given by

$$x = Q_{W1}/(Q_{W1} + Q_{W2})\,. \tag{2}$$

The induced charge pulses Q_{W1} and Q_{W2} are digitized in two ADC's (Figure 5) and the value of x is determined by means of a look-up table (Figure 6). Events are ascribed to the appropriate crystal depending from which anode preamplifier (A1 or A2) the pulse originated. Since hard solar X-rays can cause the germanium crystals to emit 9.9 keV fluorescence radiation, single-channel pulse analyzers are employed to define windows which can accept photons from the crystals (E_{max} = 6.9 keV for Fe XXVI) while rejecting the germanium fluorescence photons. A position resolution of 350 μm FWHM together with a photon energy resolution of 17% has been achieved with the SOLAR-A detectors. The former ensures good spectral resolution, while in the Fe XXVI and Fe XXV channels the uniformity of gas gain over the detector window to better than 5% allows a reduction of a factor 500 or more in the rate of processed fluorescence photons for the loss of less than 2% of the diffracted X-rays.

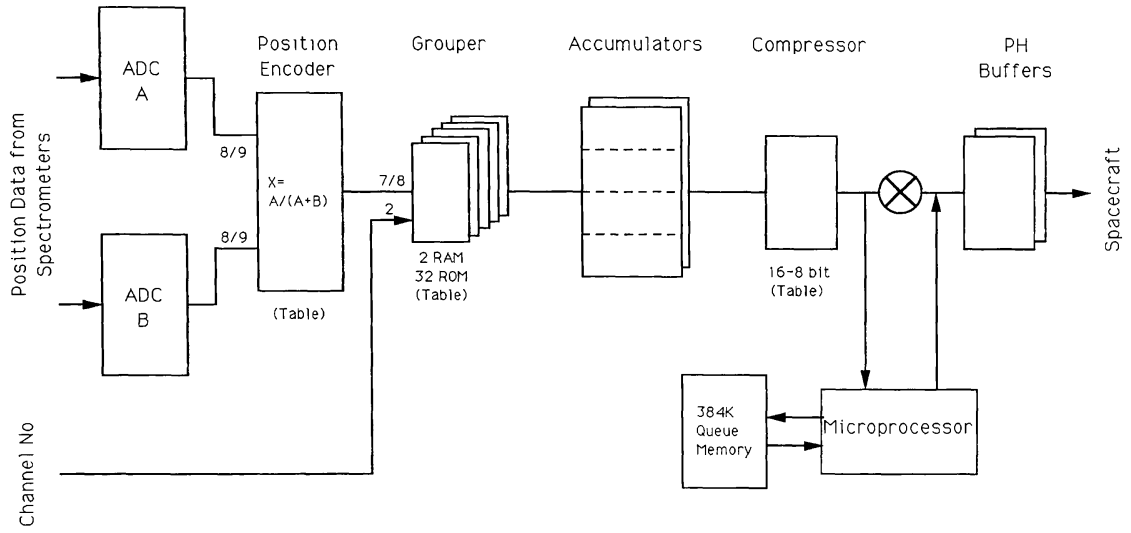

Fig. 6. The on-board data processing system. Event positions are determined in a look-up table. Spectra are assembled in the accumulators in accordance with one of the plans contained in the data grouper. The number of events in each spectral channel is compressed to an 8-bit value. Spectra can be stored in a queue memory or passed directly to buffers for the main digital data (PH) interface with the spacecraft.

5. The On-Board Processor and Data Handling

The need to acquire spectral data with good time resolution and to make optimum use of a relatively small telemetry allocation has led to the use of a sophisticated on-board data acquisition and control system which is illustrated schematically in Figure 6. Following each detected X-ray event, a pair of outputs, Q_{W1} and Q_{W2} of either 8 or 9 bits, is presented to the position encoder which is implemented as a look-up table. Using the 8-bit wavelength bin address produced by the position encoder (x in Equation (2)) together with information as to the channel of origin, an event is integrated in the accumulator. This consists of two buffers each of (4 × 256) 16-bit deep wavelength bins. This double buffer system allows data acquisition in one buffer while the other is being read out. The accumulators are sized to accommodate up to 256 bins in each channel although only 128 bins will normally be used for the Ca XIX and S XV channels. In order to optimize the number of wavelength bins used, before the event is deposited in the accumulator it is re-grouped into a 'smaller' number of bins through the use of a data grouper which is also implemented by a look-up table. Several possible grouping plans are always selectable. After the data has been accumulated for an integration period controlled by the accumulator timer, the accumulator buffers are swapped and the data is transferred from the accumulator to a hardware data compressor which is again implemented by a look-up table. Here the accumulated value of each 16-bit wavelength bin is reduced to an eight bit value before being stored in the data queue memory by the microprocessor.

Event data is output through the BCS-PH or main digital data interface to the spacecraft data processor in 256 byte blocks. The rate at which data is transferred by the interface is purely a function of the overall telemetry rate. The 384 kbyte data queue

memory allows the BCS to produce bursts of spectral data for storage at rates that are in excess of the 2 kbits s^{-1} accepted by the spacecraft telemetry system in flare mode. The amount of spectral data produced is a function of the selected data grouping plan and the accumulator integration time. The microprocessor can change the values of these parameters as a flare develops to allow a trade-off between temporal and spectral resolutions through the flare. The criteria for switching between accumulation modes and the definition of the modes themselves are contained in lists that can be loaded into the microprocessor. Since the use of the queue memory makes the PH data asynchronous to the rest of telemetry, each accumulator block in the queue is headed by a block which contains the start time and other important information.

Even rate counters (Figure 5) driven from different parts of the event control circuitry are available in the housekeeping data stream. The counters report 'total', 'in-window', and 'encoded' photons for each channel and can be used to apply deadtime corrections when the countrates are high. They are also used by the microprocessor to watch for flares and to monitor the background rate. The diagnostic PHA data used to analyze the detector performance and a field containing information generated by the microprocessor are also contained within the housekeeping data stream.

BCS electronic subsystems such as high voltage units (HVU) and single-channel analyzers (SCA) are controlled through the microprocessor data bus. Parameters may be loaded through this bus, either directly from the command interface or from the microprocessor. The value of these parameters and other information on the status of relays and switched circuitry, together with the last two received command bytes, is given in the status data stream. Structure temperatures and HV monitors are measured through the analogue data interface. In the event of a hardware problem with the microprocessor, a backup path has been provided by which spectral data flows directly from the data compressor to the BCS-PH interface. In this mode, since the data queue is not available, the number of wavelength bins produced per second must be matched to the telemetry rate by selecting an appropriate combination of the data grouping plan and accumulator integration time.

6. Instrument Calibration

Although elements of the spectrometers were calibrated and tested individually, each spectrometer was also tested end-to-end when finally assembled for flight. These tests were designed to provide a wavelength calibration and an intensity calibration at one wavelength for each of the four BCS channels.

The apparatus is shown schematically in Figure 7. The X-ray source was used to illuminate a monolithic channel-cut crystal (Quartz 1011, $2d = 6.952$ Å) which was placed about 0.8 m from the source. The channel-cut crystal was used as a two-crystal monochomator with the crystals in the $(1, -1)$ setting. Four narrow slits, two between the X-ray source and the channel cut crystal and two between the channel-cut crystal and the test chamber served to limit the beam divergence and to select the output wavelength range of the monochromator. For source radiation incident on the crystal

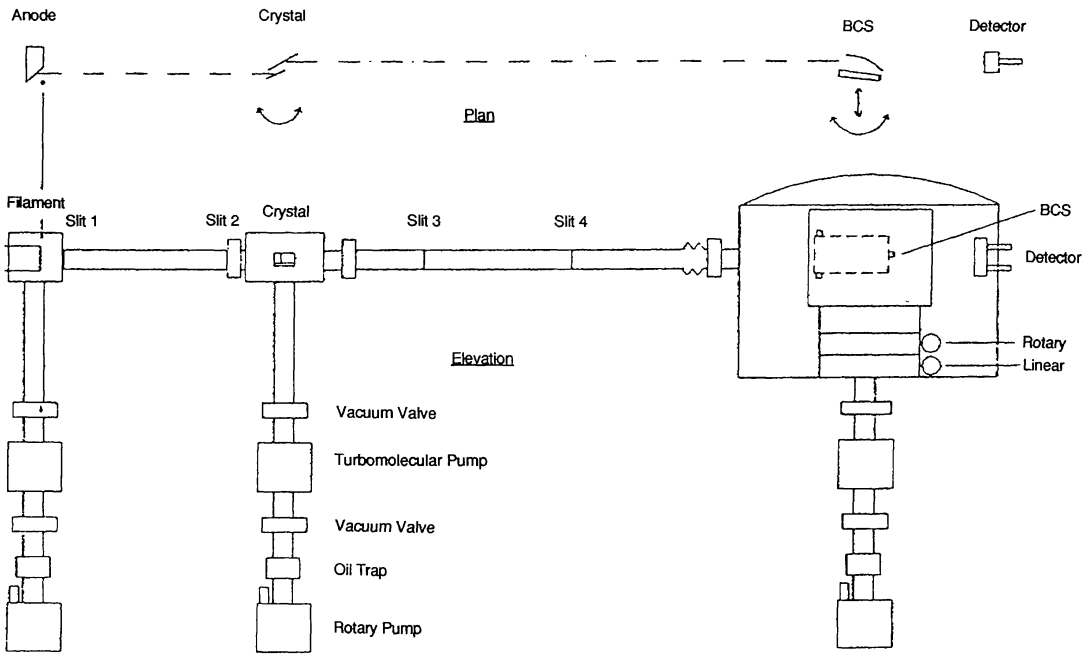

Fig. 7. The end-to-end X-ray calibration system.

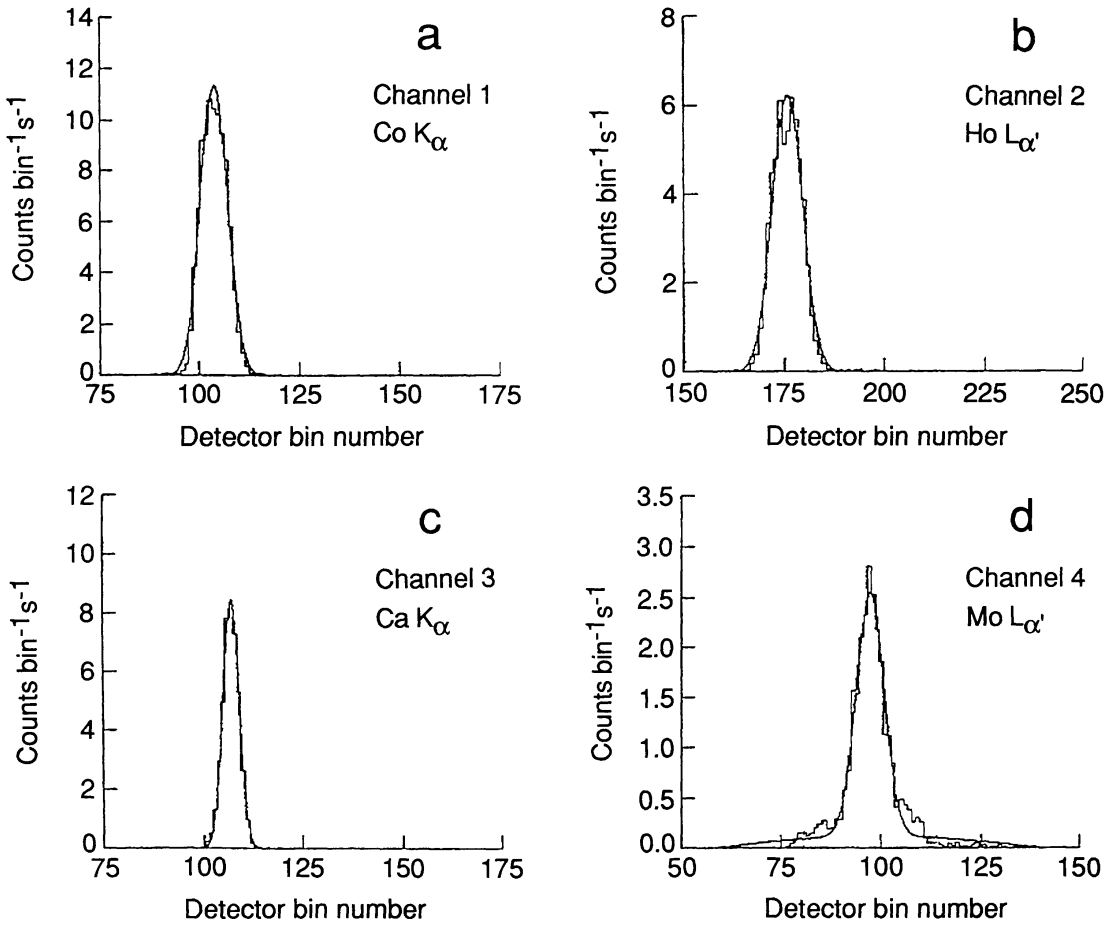

Fig. 8. Results of the end-to-end X-ray calibration of the BCS. Spectra of (a) Co $K\alpha^1$ in the Fe XXVI channel (Ch. 1), (b) Ho $L\alpha^1$ in the Fe XXV channel (Ch. 2), (c) Ca $K\alpha^2$ in the Ca XIX channel (Ch. 3), and (d) Mo $L\alpha^1$ in the S XV channel (Ch. 4).

at the correct Bragg angle for a particular Kα line, the output had the line wavelength as seen by the BCS with a profile characterized by the source linewidth, the double crystal rocking curve of the monolithic crystal and the geometry of the slits. When measured using BCS-A by rotating the instrument, the line profile had a full-width-at-half-maximum (FWHM) of around 70 arc sec for the Fe XXVI channel. The channel-cut crystal was mounted in a holder whose position was adjusted to allow changes of Bragg angle for different source wavelengths. Spectrometer units were placed about 2 m from the double crystal. The precision ground feet of each spectrometer were fixed to a vertical surface which could be moved horizontally. With the BCS aligned correctly to an X-ray beam of appropriate and known wavelength, spectral calibrations were obtained with a precision ranging from 5 mÅ for the S XV channel to better than 1 mÅ for the Fe XXVI channel. The intensity calibrations were also established with a precision of $\pm 15\%$ using a proportional counter of known quantum efficiency and geometry to interrupt the beam incident on the BCS.

For the calibration of BCS-A, lines of Co $K\alpha^1$ at 6.930 keV (1.786 Å) and Ho $L\alpha^1$ at 6.720 keV (1.842 Å) were used for the Fe XXVI and Fe XXV channels, respectively. In the case of BCS-B it was necessary to rotate the spectrometer slightly in the plane of dispersion so that lines of Ca $K\alpha^1$ at 3.691 keV (3.354 Å) and Mo $L\alpha^1$ at 2.293 keV (5.399 Å) could be used for the Ca XIX and S XV channels. The response of all four spectrometer channels to the calibration lines is indicated in Figure 8.

Acknowledgements

We gratefully acknowledge the role of the Japanese Institute for Space and Astronautical Science (ISAS) who are responsible for the SOLAR-A mission and who made it possible for the BCS team to participate in this unique study of the solar flare phenomenon. We have had through all phases of the programme the help of many colleagues at the Mullard Space Science Laboratory, the National Astronomical Observatory of Japan, the US Naval Research Laboratory (NRL), the Rutherford Appleton Laboratory, the US National Institute for Standards and Technology and of course ISAS. To all of them we give our sincere thanks. The UK groups acknowledge the support of the Science and Engineering Research Council and the British National Space Centre. The Japanese activities were made possible by the support of the grant-in-aid for International Scientific Research Program No. 63044163 and No. 01044044 of the Japanese Ministry of Education, Science and Culture. Work in the U.S.A. was supported by the US Naval Research Laboratory.

References

Acton, L. W., Culhane, J. L., Gabriel, A. H., Bentley, R. D., Bowles, J. A., Firth, J. G., Finch, M. L., Gilbreth, C. W., Guttridge, P., Hayes, R. W., Joki, E. G., Jones, B. B., Kent, B. J., Leibacher, J. W., Nobles, R. A., Patrick, T. J., Phillips, K. J. H., Rapley, C. G., Sheather, P. H., Sherman, J. C., Stark, J. P., Springer, L. A., Turner, R. F., and Wolfson, C. J.: 1980, *Solar Phys.* **65**, 53.

Acton, L. W., Culhane, J. L., Gabriel, A. H., Wolfson, C. J., Rapley, C. J., Phillips, K. J. H., Antonucci, E., Bentley, R. D., Hayes, R. W., Joki, E. G., Jordan, C., Kayat, M., Kent, B. J., Leibacher, J. W., Nobles, R. A., Parmar, A. N., Strong, K. T., and Veck, N. J.: 1981, *Astrophys. J.* **244**, L137.

Antonucci, E., Gabriel, A. H., and Dennis, B. R.: 1984, *Astrophys. J.* **287**, 917.

Antonucci, E., Gabriel, A. H., Acton, L. W., Culhane, J. L., Doyle, C. J., Leibacher, J. W., Machado, M. E., Orwig, L. E., and Rapley, C. G.: 1982, *Solar Phys.* **78**, 107.

Culhane, J. L., Gabriel, A. H., Acton, L. W., Rapley, C. G., Phillips, K. J. H., Wolfson, C. J., Antonucci, E., Bentley, R. D., Catura, R. C., Jordan, C., Kayat, M., Leibacher, J. W., McWhirter, P., Parmar, A. N., Sherman, J., Springer, L. A., Strong, K. T., and Veck, N. J.: 1981, *Astrophys. J.* **244**, L141.

Doschek, G. A.: 1983, *Solar Phys.* **86**, 9.

Doschek, G. A., Feldman, U., Kreplin, R. W., and Cohen, L.: 1980, *Astrophys. J.* **239**, 725.

Doyle, J. G. and Bentley, R. D.: 1987, *Astron. Astrophys.* **155**, 278.

Feldman, U., Doschek, G. A., Kreplin, R. W., and Mariska, J. T.: 1980, *Astrophys. J.* **241**, 1175.

Fludra, A., Lemen, J. R., Jakimiec, J., Bentley, R. D., and Sylwester, J.: 1989, *Astrophys. J.* **344**, 991.

Kondo, I.: 1982, *Hinotori Symposium on Solar Flares*, ISAS, Tokyo, p. 3.

Lin, R. P., Schwartz, R. A., Pelling, R. M., and Hurley, K. C.: 1981, *Astrophys. J.* **251**, L109.

Rapley, C. G., Culhane, J. L., Acton, L. W., Catura, R. C., Joki, E. G., and Bakke, J. C.: 1977, *Rev. Sci. Inst.* **48**, 1123.

Švestka, Z., Stewart, R. T., Hoyng, P., Van Tend, W., Acton, L. W., Gabriel, A. H., Rapley, C. G., Boelee, A., Bruner, E. C., de Jager, C., Lafleur, H., Nelson, G., Simnett, G. M., Van Beek, H. F., and Wagner, W. J.: 1982, *Solar Phys.* **75**, 305.

Sylwester, J.: 1987, *Artificial Satellites/Space Phys.* **22**, 17.

Sylwester, J., Lemen, J. R., and Mewe, R.: 1984, *Nature* **310**, 665.

Tanaka, K.: 1987, *Publ. Astron. Soc. Japan* **39**, 1.

Tanaka, K., Watanabe, T., Nishi, K., and Akita, K.: 1982, *Astrophys. J.* **254**, L59.